Accepted Manuscript

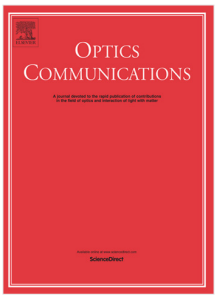

Analysis of aberrations and performance evaluation of adaptive optics in two-photon light-sheet microscopy

Caihua Zhang, Wenqiang Sun, Quanquan Mu, Zhaoliang Cao,
Xingyun Zhang, Shaoxin Wang, Li Xuan

PII: S0030-4018(18)30928-3
DOI: https://doi.org/10.1016/j.optcom.2018.10.053
Reference: OPTICS 23570

To appear in: *Optics Communications*

Received date : 20 August 2018
Revised date : 7 October 2018
Accepted date : 28 October 2018

Please cite this article as: C. Zhang, et al., Analysis of aberrations and performance evaluation of adaptive optics in two-photon light-sheet microscopy, *Optics Communications* (2018), https://doi.org/10.1016/j.optcom.2018.10.053

Analysis of aberrations and performance evaluation of adaptive optics in two-photon light-sheet microscopy

Caihua Zhang[1,2], Wenqiang Sun[1,2], Quanquan Mu[1,*], Zhaoliang Cao[1,*], Xingyun Zhang[1], Shaoxin Wang[1], Li Xuan[1]

[1]*State Key Lab of Applied Optics, Changchun Institute of Optics, Fine Mechanics and Physics, Chinese Academy of Sciences, Changchun, Jilin, 130033, China*
[2]*University of Chinese Academy of Sciences, Beijing, 100049, China*

** Corresponding author.*
E-mail addresses: muquanquan@ciomp.ac.cn (Quanquan Mu), caozlok@ciomp.ac.cn (Zhaoliang Cao)

Abstract: Two-photon light-sheet microscopy (TP-LSM) system performance is greatly degraded by specimen-induced aberrations in illumination path, which limit the field of view, axial resolution and excitation efficiency of the system. Adaptive optics (AO) is an effective method for attenuating these effects. For the design and evaluation of an AO system, a comprehensive analysis of the effects of aberrations is needed. In this paper, a TP-LSM system is simulated and new indexes based on integral intensity are introduced for the evaluation of an aberrated light sheet. Then, the influences of each Zernike mode and random aberrations on the illumination path of the TP-LSM system are investigated with a numerical simulation method. Results show that high-order aberrations have little effect on the axial resolution and excitation efficiency of the system and only low-order components require correction. The random aberrations varied in strength with the depth of the specimens, so the number of corrected Zernike modes is variable. A general formula is generated for the estimation of the number of modes that should be detected and corrected under different aberrations and different numerical aperture of the objective. The results can provide important guidance in the design and evaluation of AO units for TP-LSM systems.

***Keywords*:** Adaptive optics; Aberration correction; Two-photon Light-sheet Microscopy

1. Introduction

The optimization of biological microscopy system parameters, such as penetration depth, field of view (FOV), acquisition speed and photodamage are crucial to the progress of modern life science. However, achieving these objectives in a single type of microscopic imaging system is currently challenging as optimizing one of these parameters may degrade the others. Two-photon light-sheet microscopy (TP-LSM) systems combine the advantages of different microscopy systems. TP-LSM systems use ultrafast near-infrared laser pulse to create a two-photon excitation light sheet, simultaneously achieving high imaging depth into biological tissues and high imaging speed with low phototoxicity and photobleaching [1, 2].

A traditional light-sheet microscope illuminates a biological sample with a thin light sheet of visible light from the side of the sample. The light sheet is imaged by a wide-field camera oriented orthogonally to the sheet. Given the orthogonal geometry of a light-sheet microscope, the whole light path contains two basic parts: the illumination path and the detection path. Meanwhile, a TP-LSM system uses ultrafast near infrared laser pulse instead of visible laser to create a two-photon excitation light sheet [1] and offers a submicron-scale axial resolution unlike a tradition light sheet microscope, which is limited to 2–8 μm axial resolution.

However, similar to other microscopy systems [3, 4], TP-LSM systems are affected by aberrations introduced by biological specimens and the two orthogonal light paths of the system are affected differently. Introducing adaptive optics (AO) to biological microscopy systems is one of the approaches

for addressing such aberrations. Similar to AO technologies used in astronomical telescopes, specific wavefronts generated by wavefront correctors are used for offsetting decreased performance due to aberrations.

Over the past two decades, numerous adaptive optical microscopy systems have been implemented [5-8]. The AO technique has been widely used in two-photon microscopy [9-11] and light-sheet microscopy [12-14] for the past five years. Various detection and correction methods are applied to different systems, and many of them are of great value, such as fluorescent guide star [15], scanning technique, and descanning technique [16]. However, in the field of biological microscopic imaging, biological specimens are multifarious, and the modes of construction and principles of existing systems greatly vary. Accordingly, the extent of performance degradation due to sample-induced aberrations vary among different systems.

The detection path of a TP-LSM system is the same as that of traditional light-sheet microscope or any other plane imaging system. AO has been successfully applied to the illumination paths [17] and detection paths [12, 13] of traditional light-sheet microscopes. However, how aberrations affect the illumination path of the TP-LSM is unclear because two-photon absorption occurs in this path and the quadratic dependence on the excitation laser intensity of two-photon-excited fluorescence make the influence of the aberrations on the illumination path markedly different from that in the traditional one. In TP-LSM system, the illumination path is of vital importance because it determines the FOV and the axial resolution of the system. Knowledge about how aberrations affect the illumination path is crucial to adaptive optical design. This knowledge can be used for determining the appropriate number of Zernike modes that needs correction, actuators that a corrector should contain, and sub-apertures that must be included by the Shack-Hartmann wavefront sensor (S-H WFS), which are the most important parameters of an adaptive optical system.

In this paper, we focus on aberrations in the illumination path of a TP-LSM system and analyze the effects of the aberrations by using simulation method. Based on the point spread function (PSF) of the TP-LSM system, the two-photon light sheet is simulated and two new evaluation indexes based on integral intensity are proposed. Then, we examine the effects of each individual Zernike mode of the aberrations and different strengths of random aberrations on the illumination path. The characteristics of the influence are clear, the number of Zernike modes that requires correction is determined, and a general formula is produced. These results provide guidance for adaptive optical design and aberration correction in TP-LSM systems.

2. Methods

2.1 Optical structure of TP-LSM.

The schematic diagram of fundamental TP-LSM system is shown in Fig. 1. In the illumination path, the ultrafast near-infrared femtosecond pulse laser is emitted by a femtosecond laser source and is directed into the scan system employing axial (*x*-direction) and lateral (*y*-direction) scanning before entering the scan lens (SL), tube lens (TL), and the rear pupil of the illumination objective (IO). In the detection path, the detection objective (DO), TL, and sCMOS camera are carefully aligned for the recording of the fluorescent signal excited by the illuminating laser.

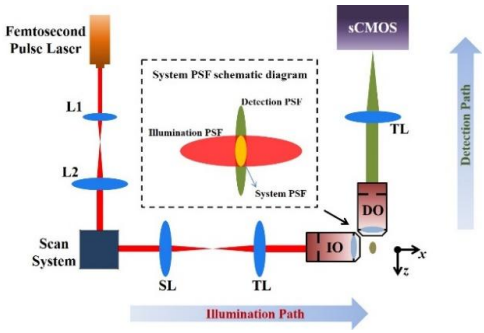

Fig. 1. Schematic diagram of the TP-LSM system.

In TP-LSM system, the virtual light sheet is generated by scanning in two directions and exposed by the sCMOS camera vertically. Compared with two-photon microscopy (TPM), TP-LSM achieves larger FOV, lower photodamage, and higher acquisition speed without causing obvious degradation in spatial resolution. However, the illumination FOV of a TP-LSM system cannot reach the desired requirement at high resolutions owing to the aberrations in the system's illumination paths.

As shown in Fig. 2, aberrations are induced as light passes through the specimen because of the variations in refractive index. In the illumination path, aberrations are induced by region "a" in the specimen. By contrast, aberrations are induced by region "b" in the detection path. The two mutually perpendicular light paths suffer from different aberrations induced by biological specimens, and the aberrations in different paths have varied influences on the system. In TP-LSM, axial resolution results from the thickness of the light sheet, and lateral resolution is determined by detection optics [1]. Aberrations in the illumination path increases the thickness of the light sheet and decreases the intensity, thus decreasing the axial resolution of the system and limiting the effective illumination FOV as illumination depth increases. Thus, the influences of aberrations on the illumination path can be investigated quantitatively by evaluating thickness and intensity of the two-photon light sheet.

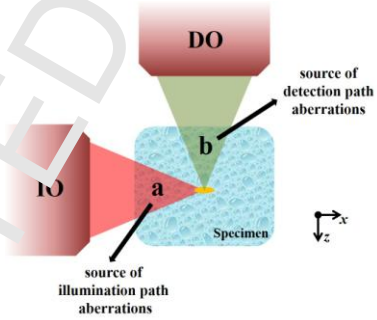

Fig. 2. Source of aberrations in different light path.

2.2 Formation of two-photon light sheet.

PSF must be calculated for the simulation of the two-photon light sheet. The system PSF of TP-LSM is calculated as follows:

$$PSF_{sys} = PSF_{ill} \times PSF_{det} \tag{1}$$

where PSF_{sys}, PSF_{ill}, and PSF_{det} represent the system PSF, illumination PSF, and detection PSF respectively. As shown in the inset of Fig. 1, PSF_{sys} is determined by the width of PSF_{ill} and PSF_{det} in the shown *x*-*z* plane. In this study, we solely focus on PSF_{ill}. The calculation method is provided below [18].

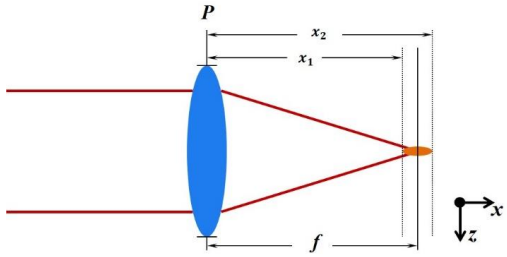

Fig. 3. The sketch map of light focused by a converging lens.

The parallel light is focused by objective lens of focal length f, as shown in Fig. 3. According to the Fresnel diffraction formula, the distribution $U_x(y,z)$ near the back focal plane of the lens can be written as

$$U_x(y,z)=\frac{\exp[j\frac{k}{2x}(y^2+z^2)]}{j\lambda x}\times\iint U_l^{'}(u,v)\exp[j\frac{k}{2x}(u^2+v^2)]\exp[-j\frac{2\pi}{\lambda x}(uy+vz)]dudv \tag{2}$$

where x is the distance from the lens to the imaging plane. A constant phase factor has been dropped. Meanwhile, $U_l^{'}(u,v)$ is the amplitude distribution behind the lens and is written as

$$U_l^{'}=U_l(u,v)P(u,v)e^{i\phi(u,v)}\exp[-j\frac{k}{2f}(u^2+v^2)] \tag{3}$$

where $U_l(u,v)$ is the disturbance incident on the lens, $\phi(u,v)$ is the aberrations in the pupil plane, and $P(u,v)$ is the pupil function. By changing the distance x from x_1 to x_2, the amplitude distribution of the focus point along the *x-axis* can be obtained. The intensity distribution can be written as

$$I_{x_1\to x_2}=U_{x_1\to x_2}(y,z)\times U_{x_1\to x_2}(y,z)^* \tag{4}$$

For the two-photon excitation, the intensity of the detected fluorescence is

$$I_f=\kappa\delta_2\eta I^2 \tag{5}$$

where κ is the collection efficiency of the imaging device, δ_2 is the two-photon cross-section, and η is the fluorescence quantum efficiency. Thus, the 3D effective illumination point spread function PSF_{ill} can be expressed as

$$PSF_{ill}(x,y,z)=\kappa\delta_2\eta I^2_{x_1\to x_2}=\kappa\delta_2\eta[U_{x_1\to x_2}(y,z)\times U_{x_1\to x_2}(y,z)^*]^2 \tag{6}$$

After the effect of the detection camera is considered, the intensity is integrated along the y-axis.

$$I_{camera}(x,z)=\int PSF_{ill}(x,y,z)dy \tag{7}$$

The virtual light sheet is scanned along the x-axis, and the intensity distribution of the two-photon light sheet can be written as

$$I_{light-sheet}(z)=\int I_{camera}(x,z)dx=\iint PSF_{ill}(x,y,z)dydx \tag{8}$$

2.3 Aberration description for TP-LSM.

In the adaptive optical system, the corrector is usually controlled with the slopes acquired by the S-H WFS. For convenience, the aberration decomposition is described by using the Zernike polynomial to express the aberrations. Therefore, the measured slopes should be transformed to the

coefficients of the Zernike polynomial. In the TP-LSM system, we use the same method to simulate the aberrations caused by specimens. The aberrations may be expressed as [19]

$$\phi(u,v)=\sum_{n=0}^{\infty}\sum_{m=0}^{n}a_{nm}Z_n^m(u,v)=\sum_{n=0}^{l}\sum_{m=0}^{n}a_{nm}Z_n^m(u,v)+\varepsilon \tag{9}$$

where Z_n^m is the orthonormal Zernike polynomial, ε is the residual error, a_{nm} is the corresponding coefficients, n and m are positive integers (including zero), and $n-m\geq 0$ and even. The index n represents the radial order, and m may be called the azimuthal order. By substituting Eq. (9) into Eq. (2) and Eq. (8), we can get the aberrated amplitude distribution of the illumination laser and the aberrated two-photon light sheet.

3. Results

The influence of aberrations on the illumination path of the TP-LSM is investigated by performing a series of simulations. We simulate the formation of the two-photon light sheet on the basis of the integral effect of a camera and the Fourier transforming properties of objective lens. Assuming that the amplitude distributions of aberrations at different depths are uniform, we obtain the aberrated light sheet in the *x*-*z* plane. Our study focuses on the simulation and analysis of the aberrated light sheet, manifested in the effects of each Zernike mode and the random aberrations caused by biological specimens**.** All the simulations only apply to the systems that scan the beam in the lateral and axial direction.

In the simulation, the equivalent focal length of the objective (f) is set to 5 mm, and the effective aperture (d) is changed. These steps ensure that different illumination numerical apertures (NA_{ill}) are obtained. The wavelength of the femtosecond pulse laser is set to 1000 nm. The tip/tilt and defocus aberrations are removed from the wavefronts in the simulations because they can only reposition the light sheet instead of distorting it.

3.1 Simulation and evaluation index of two-photon light sheet.

The distribution of illumination laser intensity (PSF_{ill}) along the beam propagation direction (*x*-axis) is simulated according to the Fourier transforming properties of converging lens and the parameters above, as shown in Fig. 4(a). The effect of the detection camera is considered in the integration of intensity along the *y*-axis. In TP-LSM, the light sheet is formed by *x*-*y* scanning. Here, we simulate the scanning of *x*-axis and obtain a virtual aberration-free light sheet at the *x*-*z* plane. Similarly, the intensity is integrated along the *x*-axis as the scanning is sequential. When induced into the system, the aberrations play a great part in PSF_{ill} and detected light sheet. A randomly aberrated wavefront is shown in Fig. 4(b). The peak to valley (PV) and root mean square (RMS) of the aberrated wavefront are 2.76λ and 0.51λ, respectively. With the effect of the aberration, the PSF_{ill} is distorted, the thickness of the generated light sheet is increased, and the intensity of fluorescence is decreased dramatically (Fig. 4(c)).

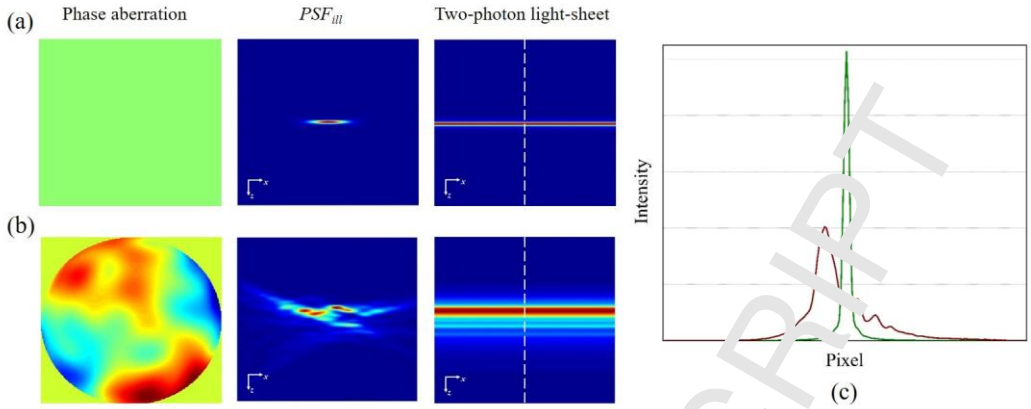

Fig. 4. The two-photon light-sheet simulation: (a) aberration-free phase, PSF_{ill}, and light sheet; (b) aberrated phase, PSF_{ill}, and light sheet; (c) Intensity distribution of the two light sheets along the *z-axis*.

In TP-LSM, the thickness of the light sheet determines the axial resolution of the system. With the thickening of the light sheet, the axial resolution decreases and the intensity is quadratically reduced, both leading to a limited FOV. To describe the influences of aberrations on axial resolution quantitatively, we define an evaluation index, which is the ratio between aberrated thickness and aberration-free thickness (*TR*) of the two-photon light sheet.

$$TR = \frac{T_A}{T_0} \tag{10}$$

where T_A and T_0 represent the thickness of aberrated and aberration-free light sheet, respectively. *TR* refers to the extent of the impact caused by aberrations. The larger the TR is, the worse the effect of the aberration is. When the TR reaches 1, the aberration has no effect on the thickness of the light sheet and on the axial resolution of the TP-LSM system.

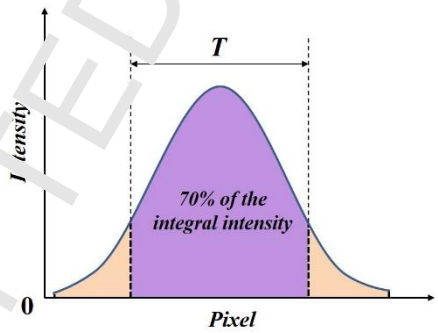

Fig. 5. Definition of the thickness *T*.

It's important to note that the full width at half maximum (FWHM) of the intensity distribution inaccurately describes the thickness of the aberrated light sheet because the distribution curve of intensity may be distorted. Thus, we define a new parameter *T* as the thickness of light sheet. The parameter *T* is the minimum width at 70% integral intensity, as shown in Fig. 5, and is equal to the FWHM of the two-photon light sheet in an aberration-free system. It can indicate the thickness of the aberrated light sheet in biological specimens accurately.

Similarly, the intensity of the light sheet indicates the excitation efficiency. To describe the influences quantitatively, we define another evaluation index: the ratio of aberrated intensity to aberration-free intensity (*IR*) of the two-photon light sheet, written as

$$IR = \frac{I_A}{I_0} \tag{11}$$

where I_A and I_0 represent the integral intensity of aberrated and aberration-free light sheet along the *z*-axis, respectively. Similar to the Strehl ratio, the smaller the IR is, the worse the effect of the aberration is. When the IR reaches 1, the aberration has no effect on the excitation efficiency of the TP-LSM system.

3.2 Effects of each Zernike mode.

Considered the two-photon absorption effect, the first 27 Zernike modes and their distortion effects along *x*-axis are calculated and shown in Fig. 6. In this section, the amplitude of aberration is appropriate to evaluate the aberration as it is specific and just contains one mode.

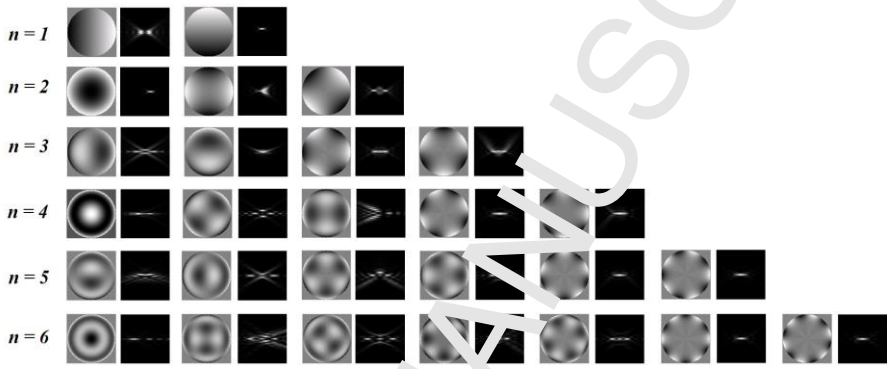

Fig. 6. The first 27 Zernike modes. For each mode, the distorted two-photon PSF_{ill} along the propagating direction is shown. All results are calculated for amplitude of 2.0 λ and *n* is the radial frequency of the aberration.

In the distorted PSF_{ill}, different Zernike modes have varied effects on axial intensity distribution. That is, different Zernike modes play different roles in the thickness and intensity of two-photon light sheet. To quantificationally analyze the differences, we investigate the effects of the first 104 modes. For each mode, a series of amplitudes from 0.5 λ to 2.0 λ are investigated.

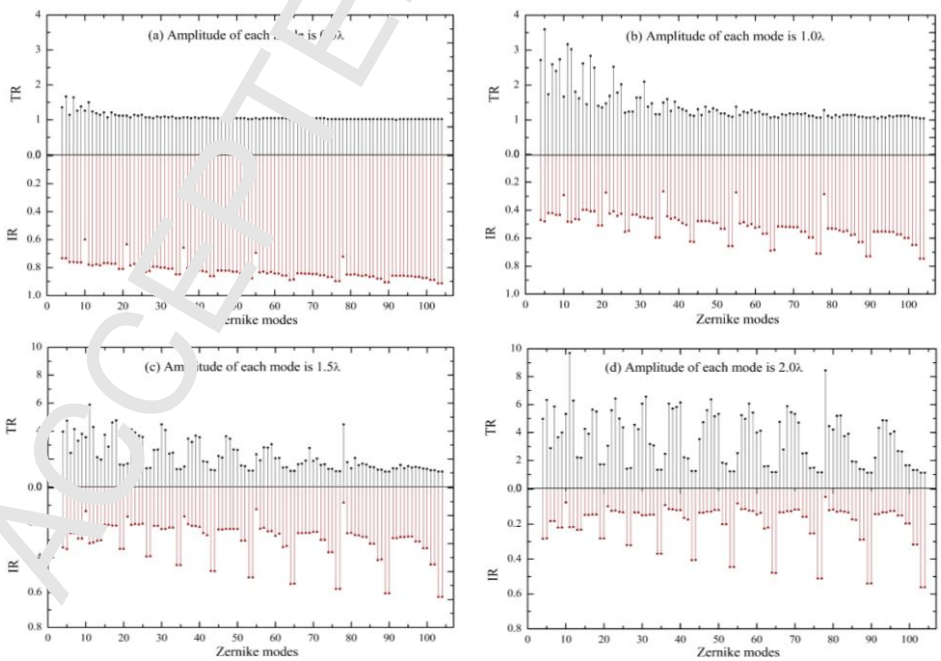

Fig. 7. Relationship between TR/IR and each Zernike mode. Amplitude of each mode is (a) 0.5λ; (b) 1.0λ; (c) 1.5λ; (d) 2.0λ.

Four representative results of the effects of different amplitudes on TR and IR are shown in Fig. 7.

First, we take the TR into account. In each Zernike mode, the greater the amplitude of the aberration is, the higher the *TR* is. Under relatively small amplitude (< 1.0 λ), the *TR* of low-order aberration is greater than that of the high-order aberration, and the high-order *TR* increases dramatically as the amplitude changes from 1.0 λ to 2.0 λ and keeps in line with the low-order *TR*. That is, the thickness of the two-photon light sheet is more sensitive to the low-order aberrations than to the high-order ones under small amplitudes. What's more, as indicated in Fig. 7(d), the aberrations affect the thickness of the light sheet regularly. In the same radial order *n*, the larger the azimuthal order *m* is, the smaller the *TR* is. When the value of *m* reaches *n* (high-order astigmatisms), the *TR* becomes extremely small.

By considering the influence on intensity, we can easily understand the inverse relationship between TR and IR. As TR become larger, IR becomes smaller and vice versa. When the two-photon light sheet becomes thicker, the dispersion of laser energy is in a relatively large area and the excitation efficiency will be reduced dramatically. However, as the figure indicates, an exception exists. The high-order spherical aberrations have little influence on the thickness of the two-photon light sheet even at a large amplitude but reduce the two-photon fluorescence intensity and degrade the image quality.

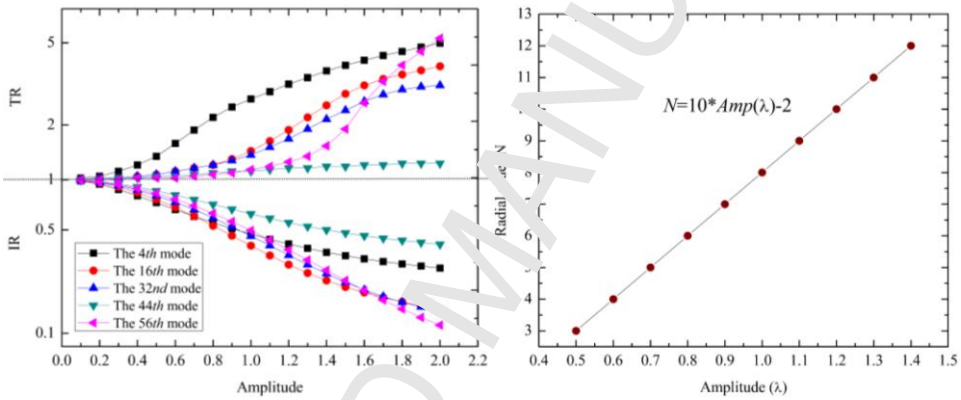

(a) (b)

Fig. 8. (a) Representatives of different modes; (b) Relationship between the amplitude *Amp* of each mode and the radial order *N* of aberration that can be more critical to improve imaging performance in the correction.

Basing on the analyses above, we conclude that the two-photon absorption effect can natively correct small-scale high-order (high radial frequency) aberrations. The importance of distorted illumination light is decreased by the quadratic dependence of two-photon excited fluorescence on the excitation light intensity as fluorophore excitation is spatially confined to only the highest intensity part of the beam, thus preserving axial resolution and fluorescence intensity even when the illumination light is distorted by aberrations. To understand the conclusion in a more precise manner, we summarize the simulations of each Zernike mode. Several representatives of different modes are provided in Fig. 8(a). At increased amplitude, different modes show different tendencies to change performance. We analyze the simulation and get the relationship between the amplitude *Amp* of each mode and the radial order *N* of aberration that can be critical to the improvement of imaging performance in the correction. The result is fitted as a linear function, as shown in Fig. 8(b). Then, the effects of each Zernike mode are summarized in Table 1. In the analysis process, we think the aberration have a severe impact if TR reaches 1.5.

Table 1. Summary of the effects of aberrations on the thickness of two-photon light sheet

	Effect on thickness	**Effect on intensity**
n-2m = 0 (spherical aberrations)	little effect	great effect

n = m (high-order astigmatisms)	little effect	little effect
n≤*N* (*N*=10**Amp*(*λ*)-2; n-2m≠0; n≠m)	great effect	great effect

3.3 Effects of random aberrations and the number of Zernike modes need to be corrected.

At every random aberrated wavefront, the amplitudes of high-order Zernike modes are usually smaller than those of the low-order ones. In the field of biological microscopy, the amplitudes of 30–60 Zernike modes at the depth of 600 μm are less than 0.5 λ [10]. So only the low order aberrations should be corrected in TP-LSM. To determine the number of Zernike modes that should be corrected, we perform another simulation.

First, aberrations induced by biological specimens are simulated by using the Zernike polynomial. To make the simulations closer to the actual situation, we use the aberration model in biological specimen proposed by M. Schwertner et al [20, 21]. The research indicates that aberrations caused by the variations in biological specimen refractive index can be approximate to random aberration. The Zernike mode standard deviation declines with rising order and this general behavior is found in all the specimens. In the adaptive optical microscopy system, we use RMS to represent the strength of the random aberrations induced by specimens at different depths as it represents the frequency character of the aberrated wavefronts. According to the results produced by Kai Wang et al [9, 10] in the zebrafish embryos and mouse cortex, the aberration is weak and RMS is approximately 0.1λ for the superficial specimen (<100 μm; λ=1000nm for the TP-LSM). For the deeper specimen, the aberration is moderate and RMS is approximately 0.5λ. When the illuminating position of the TP-LSM system goes deeper (>500 μm), the aberration is strong and RMS is approximately 1.0λ. Based on the aberration model above, 1000 wavefronts are generated randomly for each aberration strength, and the average TR and IR of the 1000 sets of wavefronts are used to obtain statistical results. The closer to 1 the TR and IR values are, the better the correction effect of the method is. The relation among TR, IR, and the number of corrected Zernike modes J under random aberration with variable strength is shown in Fig. 9.

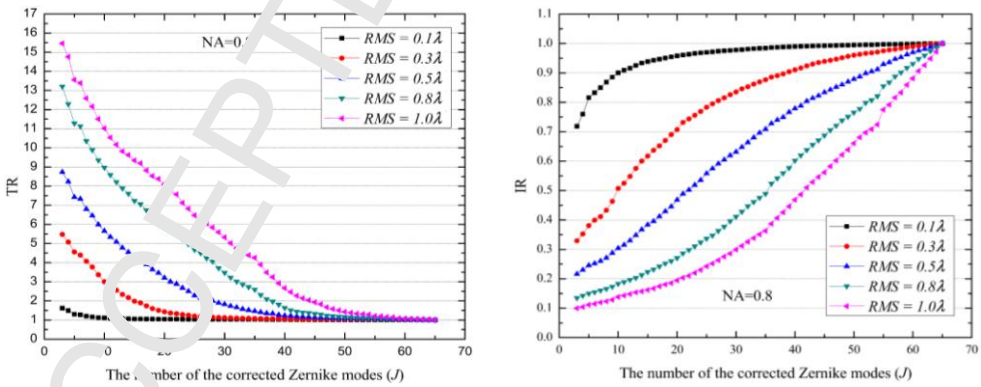

(a) (b)

Fig. 9. TR and IR of different RMS of the initial random aberration varying with the number of corrected Zernike modes. NA of the illumination objective is 0.8.

As is shown in Fig. 9(a), TR and IR change with the number of corrected Zernike modes for varying RMS of the random aberration. Practically, it can be assumed that the correction of AO unit is ideal when TR is smaller than 1.1 and IR is larger than 0.8. For weak aberration, RMS=0.1λ, the first 11 modes need to be corrected to achieve ideal correction. Considering a stronger turbulence,

RMS=0.3λ, TR is 1.09 and IR is 0.86 with 33 Zernike modes corrected. However, for moderate or strong aberration, 49 or more Zernike modes should be corrected to make it.

In TP-LSM, NA_{ill} is an important parameter. The effects of random aberrations vary among different NA_{ill} values. Fig. 10(a) illustrates the meaning of NA dependent aberrations. For the same objective, the working distance (WD) is fixed. When the illumination aperture decreases, the size of the light cone passing through the specimen decreases, and the system will suffer a more moderate aberration. To simulate this phenomenon, a single random aberration is generated for the high NA_{ill} and then cropped in the simulation of a lower NA_{ill}. The two-photon light sheets and the correction process are simulated under three different NA_{ill} (Fig. 10(b-d)). The effect is severe at high NA_{ill}, and the same correction effect can be obtained by increasing the number Zernike modes for correction.

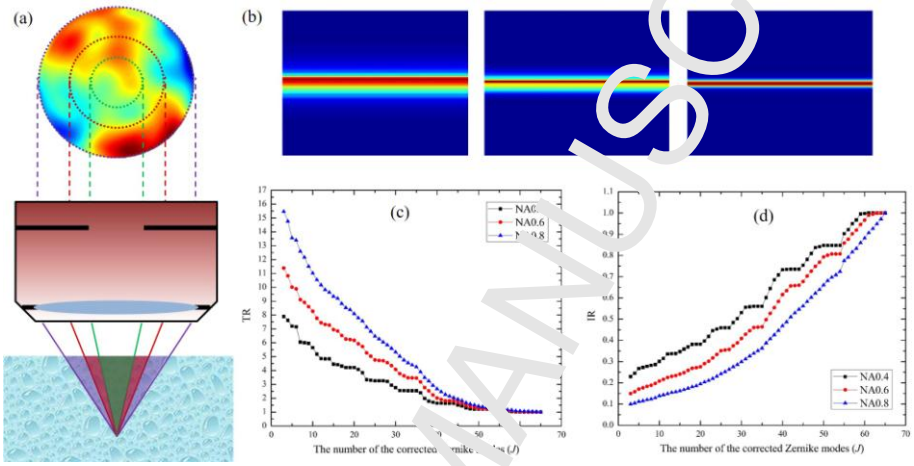

Fig. 10. (a) Illustration of NA dependent aberrations; (b) two-photon light-sheet under different NA_{ill}; (c) TR and (d) IR varying with the number of corrected Zernike modes under different NA_{ill}.

To investigate the influence more fully, we make a specific comparison of the correction process between different NA_{ill} and different strength of the random aberrations. The aberration for lower NA_{ill} is cropped from the highest one, and the corresponding RMS is changed and calculated. The detailed number variation values of corrected Zernike modes to keep TR below 1.1 and IR above 0.8 are provided in Fig. 11. To make the results more universal, we fit the points as power functions. The fitting equations are shown in the figure at the same time. With the three fitting equations, a general formula between the number of corrected Zernike modes (J), the RMS of the random aberrations, and the NA_{ill} can be made and written as

$$J = 58 \times \left[1 - \left| RMS(\lambda) - 1.03 \right|^{(2 \times NA_{ill} + 1.2)} \right] \tag{12}$$

With the general formula above, the number of Zernike modes that the AO system must detect and correct under different scales of random aberrations and different NA_{ill} values can be estimated. This formula plays a great part in the design and performance evaluation of an AO system in TP-LSM.

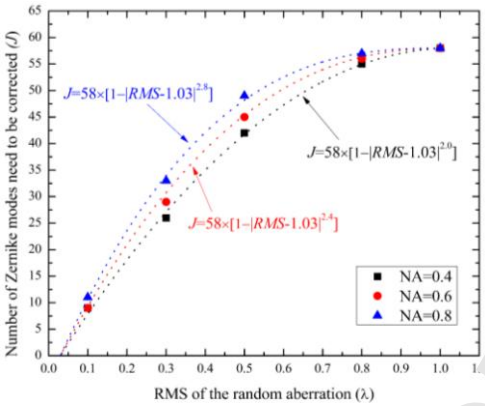

Fig. 11. Number of Zernike modes that requires correction under random aberration with variable strength and different NA of the objective.

4. Discussion

In this paper, a two-photon light sheet is simulated, and the evaluation indexes of the light sheet are proposed. The influence of aberrations on the illumination path of the TP-LSM is studied. The effects of each Zernike modes and random aberrations on the two-photon light sheet are investigated, and the relationship among the amplitude of each mode, the RMS of the random aberration, the number of the corrected Zernike modes, the NA of illumination objective, the thickness and intensity of the light sheet is derived.

Based on the relationship above, a series of results can be produced. First, in TP-LSM, the high-order aberrations have little effect on the axial resolution of the system because of the quadratic dependence on the excitation laser intensity of two-photon-excited fluorescence. Thus, only the low-order components should be corrected. Second, as the aberrations at different depths of the biological specimens vary in strength, the number of Zernike modes that needs correction is variable. Third, when the NA_{ill} gets large, the thickness of the light sheet becomes increasingly sensitive to the same aberration. This result indicates that a small NA should be used in the illumination path of TP-LSM. Fourth, a general formula is made for the estimation of the number of modes that should be corrected in different case. According to the formula, although varing with the strength of aberrations induced by the specimens and NA of the objective, the number of Zernike modes that should be corrected can be fixed at 58 even when the aberration is strong (RMS=1.0λ) and NA is large (NA_{ill}=0.8). These results will contribute to the design of wavefront sensor and corrector and the performance evaluation of AO unit for TP-LSM.

In the AO system, the sub-aperture number of S-H WFS determines the number of Zernike modes that can be measured, and the element number of corrector determines the number of Zernike modes that can be corrected. Hence, the general formula in the TP-LSM can be used in the selection of a sub-aperture number for S-H WFS and element number for the wavefront corrector. For the application of AO on the illumination path of TP-LSM, a S-H WFS with 10×10 sub-apertures is sufficient to measure 58 Zernike modes, and a deformable mirror (DM) with more than 100 actuators or a liquid crystal based light modulator (LC-SLM) should be used in the correction of aberrations.

On the basis of the conclusions above, an experimental TP-LSM system with an AO unit will be built in the future work. By applying the AO technique, a fluorescence microscopy system can achieve large FOV and high spatial resolution.

References

[1] T.V. Truong, W. Supatto, D.S. Koos, J.M. Choi, S.E. Fraser, Deep and fast live imaging with two-photon scanned light-sheet microscopy, Nature Methods, 8 (2011) 757-760.

[2] W. Zong, J. Zhao, X. Chen, Y. Lin, H. Ren, Y. Zhang, M. Fan, Z. Zhou, H. Cheng, Y. Sun, Large-field high-resolution two-photon digital scanned light-sheet microscopy, Cell Research, 25 (2015) 254-257.

[3] J. Antonello, D. Burke, M.J. Booth, Aberrations in stimulated emission depletion (STED) microscopy, Optics Communications, 404 (2017).

[4] X. Hao, J. Antonello, E.S. Allgeyer, J. Bewersdorf, M.J. Booth, Aberrations in 4Pi Microscopy, Optics Express, 25 (2017) 14049-14058.

[5] M.J. Booth, Adaptive Optics in Microscopy, Wiley-Blackwell2011.

[6] M.J. Booth, Adaptive optical microscopy: the ongoing quest for a perfect image, Light Science & Applications, 3 (2014) e165.

[7] N. Ji, Adaptive optical fluorescence microscopy, Nature Methods, 14 (2017) 374.

[8] C. Zhang, Z. Zhao, L. Chen, Z. Cao, and H. Mao, "Application of adaptive optics in biological fluorescent microscopy (in Chinese), " Sci Sin-Phys Mech Astron, 47(8), 084204 (2017).

[9] K. Wang, D.E. Milkie, A. Saxena, P. Engerer, T. Misgeld, M.E. Bronner, J. Mumm, E. Betzig, Rapid adaptive optical recovery of optimal resolution over large volumes, Nature Methods, 11 (2014) 625.

[10] K. Wang, W. Sun, C.T. Richie, B.K. Harvey, E. Betzig, N. Ji, Direct wavefront sensing for high-resolution in vivo imaging in scattering tissue, Nature Communications, 6 (2015) 7276.

[11] W. Zheng, Y. Wu, P. Winter, H. Shroff, Adaptive optics improves multiphoton super-resolution imaging, Society of Photo-Optical Instrumentation Engineers2018, pp. 36.

[12] C. Bourgenot, C.D. Saunter, J.M. Taylor, J.M. Girkin, G.D. Love, 3D adaptive optics in a light sheet microscope, Optics Express, 20 (2012) 13252-13261.

[13] R. Jorand, G.L. Corre, J. Andilla, A. Maandhui, C. Frongia, V. Lobjois, B. Ducommun, C. Lorenzo, Deep and Clear Optical Imaging of Thick Inhomogeneous Samples, Plos One, 7 (2011) e35795.

[14] S.H. Moosavi, C. Gohnkreuz, A. Rohrbach, Feedback phase correction of Bessel beams in confocal line light-sheet microscopy: a simulation study, Appl Opt, 52 (2013) 5835-5842.

[15] R. Avilesespinosa, J. Andilla, R. Porcarguezenec, O.E. Olarte, M. Nieto, X. Levecq, D. Artigas, P. Lozaalvarez, Measurement and correction of in vivo sample aberrations employing a nonlinear guide-star in two-photon excited fluorescence microscopy, Biomedical Optics Express, 2 (2011) 3135.

[16] H. Hofer, P. Artal, B. Singer, J.L. Aragón, D.R. Williams, Dynamics of the eye's wave aberration, Journal of the Optical Society of America A Optics Image Science & Vision, 18 (2001) 497-506.

[17] T.L. Liu, S. Upadhyayula, D.E. Milkie, V. Singh, K. Wang, I.A. Swinburne, K.R. Mosaliganti, Z.M. Collins, T.W. Hiscock, J. Shea, Observing the cell in its native state: Imaging subcellular dynamics in multicellular organisms, Science, 360 (2018).

[18] J.W. Goodman, M.E. Cox, Introduction to Fourier Optics, McGraw-Hill1968.

[19] M. Born, E. Wolf, Principles of Optics, Pergamon Press1959.

[20] M. Schwertner, M.J. Booth, M.A.A. Neil, T. Wilson, Measurement of specimen-induced aberrations of biological samples using phase stepping interferometry, Journal of Microscopy, 213 (2004) 11.

[21] M. Schwertner, M.J. Booth, T. Wilson, Characterizing specimen induced aberrations for high NA adaptive optical microscopy, Optics Express, 12 (2004) 6540.

Acknowledgment

This work is supported by the National Natural Science Foundation of China with grant numbers 61205021 and 11204299.